How microtubule kinetics contribute to phragmoplast assembly and expansion

Leander Schuitman
Reg. Nr.: 84 09 27 752 080
1st Supervisor: Tijs Ketelaar
2nd Supervisor: Marcel Janson
3rd Supervisor: Jelmer Lindeboom.
Chair group: Plant Cell Biology
Wageningen University

Master Biology Thesis

August 2011

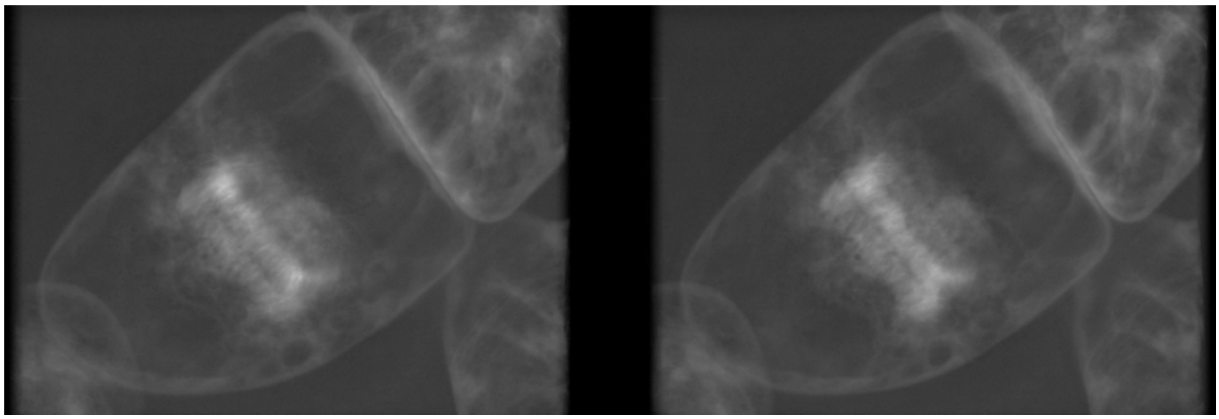

Abstract

Ever since the discovery of the cytoskeleton and microtubule (MT) dynamic instability, the relation between behaviour of these “muscles” of cells and the cellular processes have been studied. Only little of this research has been focussed on the dynamics of MT as they play their pivotal role in the division of plant cells by building the dividing cell wall precursor. We have investigated some of the established MT dynamics and connected them to the process that is so important to plant organ formation and plant growth in general. During this research we were able to make detailed, high speed records of MT growth within the solid and expanding phragmoplast and thus were able to show that phragmoplast MTs grow in an unordarly fashion and with a speed exceeding that of cortical growth. Tracing EB1 comets at growing MT plus ends revealed overlap of MTs to be present only outside of the region were diminished tubulin density indicates the presence of the CP. Furthermore we were able to confirm the expansion of the phragmoplast to be caused by addition of MTs at the centrifugal edge while EB1 comets show persistent MT growth at the inner edge of the expanding phragmoplast. Also a remarkable flux of tubulin receding the CP was found together with lateral vibration of minus ends of MTs or MT bundles. Directional FRAP experiments showed a large heterogeneity of this movement to exist within every region of the phragmoplast.

Abbreviations: CP cell plate; EB1 end binding protein 1; MT microtubule; PPB pre prophase Band.

INTRODUCTION

The cell cycle

Through the dynamic behaviour of the cytoskeletons major constituents (Brøndsted and Carlsen, 1951); the microtubules (MTs), actin filaments (AFs) and intermediate filaments (De Loof et al., 1996), it assumes different arrays in accordance to the cells needs during the different phases of the cell cycle [Pickett-Heaps 1999]. The functions of the cytoskeleton and the names of the associated arrays include, amongst others, vesicle and organelle transport (cortical array) reviewed in (Pickett-Heaps et al., 1999) chromosome segregation (spindle) (reviewed in (Tanenbaum and Medema, 2010) (Pickett-Heaps et al.)) and demarcation of the division plane (pre prophase band) reviewed in (Van Damme, 2009). An array unique to plants (Pickett-Heaps et al., 1999) is the phragmoplast. The function of this array is to build a new cell wall precursor, the cell plate, (CP) (Reichardt et al., 2007), that divides a cell in to two daughter cells. Like the present cell wall surrounding the cell this wall is very important to the cells strength [Pickett-Heaps 1999].

The phragmoplast

The MTs of the phragmoplast form two antiparallel sheaves at the same location as the spindle, in the same orientation, roughly perpendicular to the division plane. Because the phragmoplast emanates from the spindle, and the shapes of these arrays are much alike, it is hard to visually distinguish the one from the other. The CP is build-up by the fusion of phragmoplast guided vesicles, and the coagulation of the material these vesicles contain, in to a meshwork that expands centrifugally and condenses over time (Samuels et al., 1995). To facilitated the centrifugal growth the two halves of the phragmoplast change from sheaves into rings that increase in diameter till the CP formation is complete with the CP reaching the cells cortex all around. The phragmoplast guides the growing CP to the division plain marked earlier by the pre prophase band. In tobacco BY-2 cells actin is not necessary for formation and full development of the phragmoplast. The guidance of the young CP to the ring in the cell cortex that was delineated as the division site by the PPB earlier on, does not require actin either. [Yoneda et al 2004]

Evolutionary older plant taxons, like algae, exhibit a circular indentation of the cell wall around the division plane in addition to the Phragmoplast (Goto and Ueda, 1988; Sawitzky and Grolig, 1995). This furrow is analogues to the way non-plant organisms perform cytokinesis end suggests an evolutionary congeniality to these other organisms.

Cytoskeleton kinetics

The versatility and flexibility the cytoskeleton exhibits can be attributed to the way its mayor constituents: the MTs and AFs are build up. The building blocks of both filaments can easily assemble and dissociate from the filament tips hence enabling rapid changes between initiation, growth, shrinkage, pause and complete disassembly. These phases and the switching between them is called dynamic instability reviewed in (Cassimeris et al., 1987; Carlier and Pantaloni, 1997). Combined growth at one end and breakdown at a similar pace at the other end is called treadmilling. If the growing tip encounters an obstacle, tread milling results in the whole filament staying at the same location while, all of its parts move away from the obstacle. Inversely, if the building blocks are positionally fixed, the object as a whole will move during tread milling. MTs can also be moved by the action of molecular motors. When parallel MTs are forced to move alongside each other we speak of sliding (Lindemann et al., 1992). By growing, MTs can exert force on objects (Dogterom and Yurke, 1997). For the production of this force, as well as for growth without resistance energy is needed, which is supplied in the form of GTP and de-phosphorylation to GDP and phosphorus [reviewed in Cassimeris et al 1987].

This is the time.

There are many studies on MT kinetics, in different arrays, in different organisms and also in vitro, e.g. (Lindemann et al., 1992; Dogterom and Yurke, 1997; Vos et al., 2004) respectively. Yet the research truly focusing on MT kinetics in the phragmoplast, is, for as far as we are aware, limited to three publications (Asada et al., 1991; Vantard et al., 1990; Austin et al., 2005), the latter being electron microscopy research. Till recently it was not possible to visualize individual microtubules deep inside the living cell as is necessary for MT kinetics studies in either the spindle or the phragmoplast. Asada and Vantard (1991) use MT staining methods that involve manipulations of the cell as a whole and of the cytoskeletons stability in particular. The manipulations are likely to interfere with the observed MT kinetics and therefore jeopardize the reliability of the observations to accurately represent genuine in vivo dynamics. Electron microscopy necessitates cell congelation that involves cell death and possibly causes artefacts. Introduction of the spinning disk in addition to (fluorescence-) single-point laser scanning technique has improved microscopy such that we can now get well focused images at depths of several µm at a rate that allows us to follow the dynamics of individual MTs much deeper within the cell than just the proximal cortex. For this study we used genetical modification to stain MT parts, to minimalise interference with the cells viability and MT kinetics.

MATERIALS AND METHODES

BY-2 cell line

The cells used are *Bright Yellow* BY-2 *Nicotiana tabacum* cells. The line stably expressing the GFP-TUA construct was available in the PCB lab (original construct supplied by F. Kumagai [kumagai, 2001] The GFP-TUA- -mCherry-EB1 line was derived from the GFP-TUA line by agrobacterium mediated transfection with the mCherry-EB1 construct. Both lines were grown in liquid medium (see appendix 1) and on solid medium (see appendix 1). Every 7 days 4 ml old liquid culture was diluted in 36 ml fresh medium with appropriate antibiotics for constant selection. Cultures were incubated at 25^{o}C in the dark in 250 ml flasks on a horizontal shaker rotating at 100rpm. When a growth of a culture declined it was sub cultured every 14 days till it regained original density.

Calli were partially transferred to new medium when necessary, judging from callus colour, which was several month.

Transformation

A bit of a -80^{o}C glycerol stock of *Agrobacterium tumefaciens* containing a multisite gateway plasmid pMDC43 containing a 35S::mCherry::EB1 construct (Gutierrez, 2009) and harbouring basta resistance was grown on a solid selective medium. A selected colony was cultured with the GFP-TUA BY-2 cells according to the protocol in appendix 1. In the same way five more transformations were attempted (see appendix 2), these failed however.

Sample preparation

For imaging, between 30 and 40 µl of 3 to 6 days old cell suspension was pipetted on a 3x3 cm piece of biofoil (viva science, In Vitro System & service GMbH, Göttingen) that was fixed, by 70-96% ethanol evaporation, over a ca. 2 cm diameter hole in a custom made microscope slide. The drop was covered with a coverslip and medium was drained away till the cells became fixed between the foil and coverslip. Thereafter the space was sealed and the coverslip was fixed to the foil and the slide with molten valap (a 1:1:1 mixture of acid free Vaseline, lanolin and paraffin). The sample was mounted on the microscope stage with the coverslip facing downwards. Cell survival lasted up to, at least, seven days in these samples.

Microscope equipement

For imaging a *Nikon Eclipse Ti* inverted microscope equipped with a 100x 1.4 NA oil emission objective, a *Yokogwa CSU-X1* spinningdisk confocal unit and 491 nm and 561 nm lasers was used. Output was recorded on a *Photometrics evolve* EM CCD camera. Multicolour recordings were made by switching between excitation lasers. Equipment was controlled using *MetaMorph imaging software (Molecular Devices)*. FRAP was performed using a *Roper Scientific* FRAP unit controlled by *ILAS* software and plugins in *MetaMorph.*

Imaging of the phragmoplast.

For imaging and analysis the following terms are important to explain.

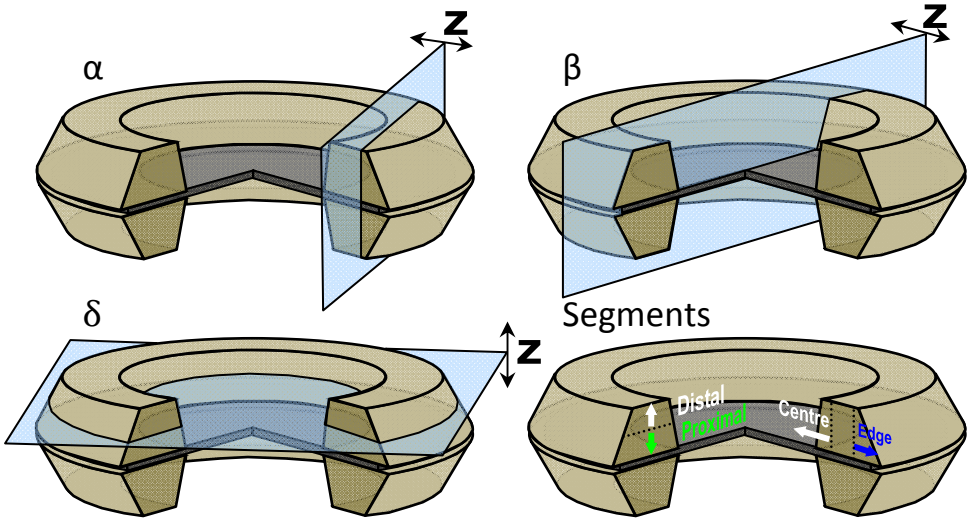

Figure 1 Confocal sections and regions within the phragmoplast. Schematic image of the phragmoplast and cell plate with one quarter cut out. In the first three images the blue planes depict a confocal slice cutting through the phragmoplast. these three ways are called α (alfa) β (beta) and δ (delta). By moving α plane towards the phragmoplast centre it becomes a β plain, the same can be true when a permanent focal position is maintained and the phragmoplast expands or moves perpendicular to the plain. In reality the confocal plains are not positioned at angle of exactly 90^{o} (α, β) or 0^{o} (δ)relative to the CP as depicted here. The fourth image depicts the regions as used in the text and for comparing FRAP analysis. For FRAP the length of the regions are Proximal/Distal 1/1, central and edge are 2µm from the respective phragmoplast edges. Cartoon and characters for for view/plains based on Hussey 2011.

Kymographs

Kymographs were made using the *multiple kymograph* plugin in *ImageJ* (*Broken Symmetry Software*). Kymographs based on nonlinear lines are used to follow and measure multiple objects e.g. comets or parts of the phragmoplast simultaneously. In these kymographs displacement of objects in the same direction does not implied similarity of direction in the recordings that the kymograph is based on. Parallel movement of objects in these kymographs implies movement at equal speeds, relative to the respective parts of the kymograph line. Wide kymographs were also made using the same tools, but necessitated a *multiple overlay* to be made of the

kymographs. In wide kymographs the intensities of pixels over a designated width (perpendicular to the length of the kymograph line) are averaged. Unless indicated otherwise kymographs lines are directed from top to bottom and from left to right. In resulting kymographs time is always directed downwards and distance along the kymograph line from left to right, regardless of the orientation of the kymograph line in the source record.

MT growth speed

MT growth speed was calculated from growth distances and time intervals during growth, inferred from kymographs of growing MTs or EB1 comets without apparent pauses or episodes of shrinkage. For calculating growth speed of phragmoplast MTs, distance and time were read from kymographs of individual comets. In the cortex the *imageJ kymo analysis* macro was used to read these parameters from kymographs of many MTs or EB1s simultaneously. The *ImageJ* plugin *stackreg>RigidBody* [Thévenaz et al. 1998] was used to stabilize one of the time lapse records.

Intensity plots

For intensity plots images were averaged in *ImageJ*. The measurements were performed using the lines scan function in *MetaMorph*. Direction, length and width of this band were chosen. All intensities measured over the width of the band were averaged. For every band background was measured and subtracted using *Excel (Microsoft office 2010)* . The remaining values were made comparable by dividing them by the maximum value within every band. Graphs were made in excel.

Statistics

X^2 test were performed using *Excel*, other comparitive statistical test were performed using *SPSS statistics 19* software (*IBM*). Meanvalues and standard errors were calculated using the *Descriptive statistics* function of the *data analysis* plugin in *Excel*. Histograms were made in *Excel* using the *histrogram function* of the same plugin.

Simulated convolution

Convolution simulations were performed using *Excel* and *Origin 8.5 (OriginLab Corporation, One Roundhouse Plaza, Northampton USA).* Presumed linear profiles and linear convolution distributions were made in *Excel* and copied into Origin. Convolution distribution function was

$$\left[\frac{\sin\left[\frac{\pi \cdot x}{\frac{(0.5 \cdot 1.22 \cdot \lambda)}{na}}\right]}{\left[\frac{\pi \cdot x}{\left(\frac{0.5 \cdot 1.22 \cdot \lambda}{na}\right)}\right]}\right]^2$$

With x being the consecutive points in the sample, n.a. being numerical aperture=1.4, λ in nm and x being the distance to every point, calculated for every 100 nm over a width of 400nm. To standardize the output for every wavelength the resulting values were divided by their respective sum. The function *signal processing>convolution* in Origin was used to convolve the presumed intensity distributions with the standardized convolution distributions. Graphs of the output were made in Excel.

RESULTS

Introduction mCherry-EB1

To monitor MT dynamics, we need to be able to distinguish MTs from one another. Especially for recording Growths speed and direction plus ends of individual MTs need to be tracked. Within the phragmoplast individual MTs often can not be distinguished because of their high density however. To overcome this problem we introduced a construct containing the genes for the red fluorescing mCherry linked to MT plus end tracking protein EB1, into the present GFP-TUA line. This transfections resulted in one viable callus culture, of which almost all of the derived suspension culture cells expressed both GFP-TUA and mCherry-EB1. The remaining cells expressed only GFP-TUA. The culture expressing both constructs will be revered to as GFP-TUA_mCherry-EB1 henceforth. The viability of the GFP-TUA_mCherry-EB1 line in suspension was good and comparable to the GFP-TUA line. In the GFP-TUA_mCherry-EB1 cells, dots or patches of a red signal (comets) were observed at the growing plus end of MTs (see figure 2). This is as expected and described earlier in (Akhmanova and Hoogenraad; Akhmanova and Steinmetz).In the kymographs of figure 2 the EB1 can be seen tracking the ends of growing MTs.

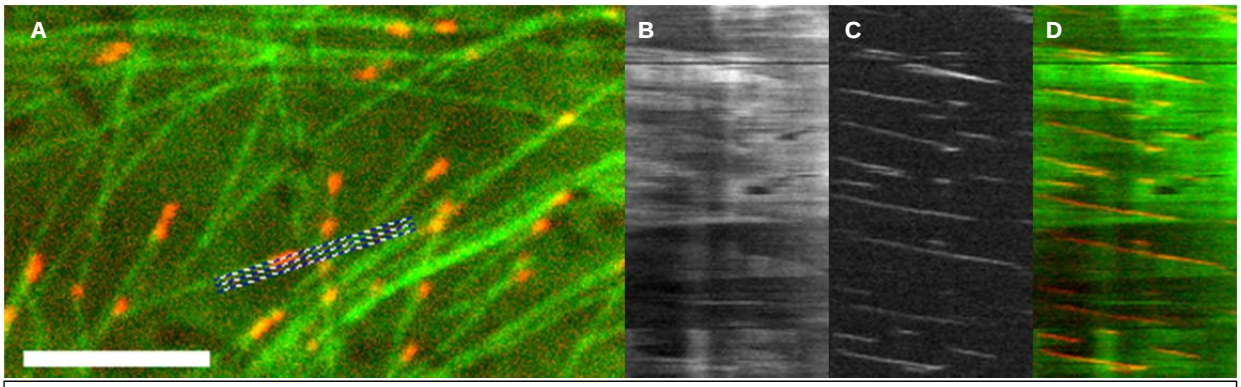

Figure xxx004: **A)** snapshot of a cell expressing GFP-TUA (green) and mCherry-EB1(red) cell cortex with growing MTs. **B,C,D)** kymographs of the corresponding movie, along the dashed lines in A (width = 7 pixels) . **B)** GFP-TUA. **C)** mCherry-EB1. **D)** composite of B and C. total time is 20 min and 51.4 sec. scale bar = 5 µm for A-D.

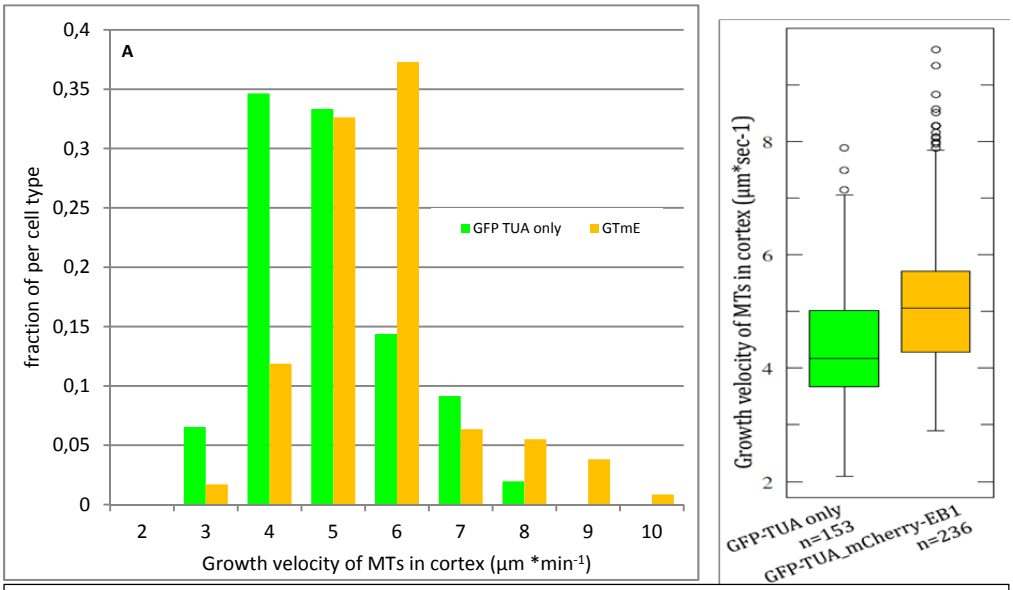

Figure 3 MT growth speed distributions in the cells cortex. **A)** Histogram of velocities. **B)** Graphical representation of Average speed in GFP-TUA and GFP-TUA_mCherry-EB1 cells. Bars show standard deviations.

Possible influence of MT dynamics by the overabundance of the growth stimulating EB1 as a result of expression of the new mCherry-EB1 construct was examined by measuring and comparing the growth speed of

MTs in the cortex of the GFP-TUA and GFP-TUA- -Cherry-EB1 cells. Distributions of speed are depicted in figure 3. Growth speed was lower in the GFP-TUA cells than it was in GFP-TUA_mCherry-EB1 cells ($p<0.01$. (independent samples Mann Whitney U test) with mean velocities of 4.4 (SE= 0.095) and 5.2 µm*sec^{-1} (SE= 0.085) respectively. Ratios between growth per area or growth of total length of MTs was not measured.

FLUORESCENSE INTENSITY AND CP WIDTH

Because literature presents us with conflicting statements regarding the presumed overlap and interdigitation of the MTs of the two phragmoplast halves Assaad et al., [2001], Shopfer and Hepler [1991] and Segui Simaro et al., [2004] we looked at GFP intensity distribution.

The GFP signal intensity is not uniformly distributed over the phragmoplast. (see fig. 4**).** Roughly in the middle a dark line can be distinguished. This is opposite to the pattern expected for interdigitation, were an elevation of fluorescence should be present in the regions were MT overlap.

A total absence of MTs in this darker region cannot be concluded, as the fluorescence intensity here is still high relative to the rest of the cell outside of the phragmoplast. Probably the light in this band is a result from light scattering from the phragmoplast, like the light in the vacuole surrounding the phragmoplast as can be seen clearly in figure 4 D,E.

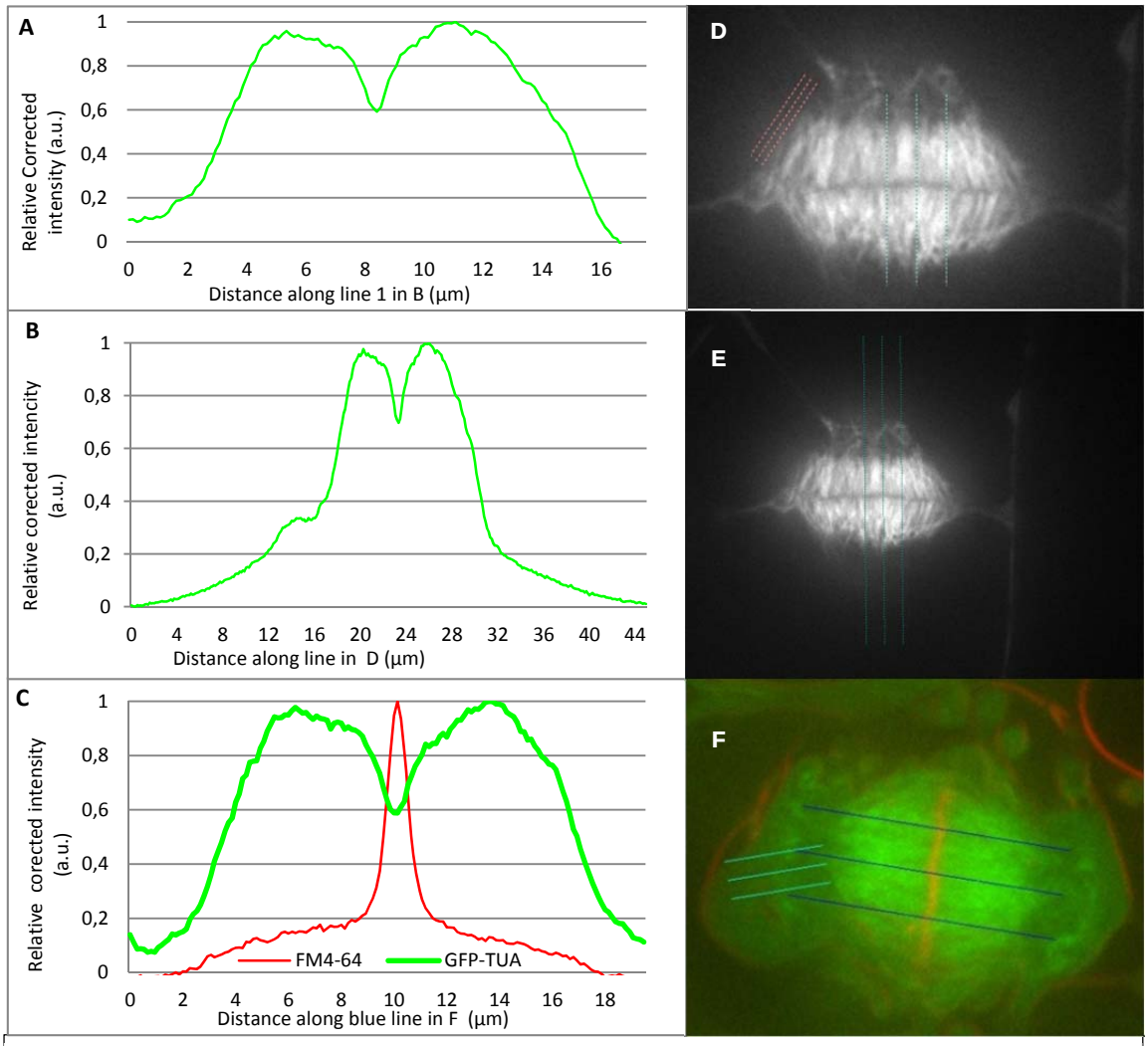

Figure 4 Intensity plot across (α views of) phragmoplast.

A-C) GFP-TUA fluorescence intensity plots across the phragmoplast in D-F. Values are the fraction of the maximum , calculated after subtraction of the background signal. A dent in the fluorescence intensity is visible. In C it coincides with the red FM4-64 peak. B shows an increased in fluorescence surrounding the phragmoplast **D-F)** Snapshots of phragmoplast of GFP-TUA cell. In F membranes (of the developing CP) are stained with FM4-64. Blue (dashed) lines indicate intensity measurement regions for A,C,E. Red and cyan lines in D and F indicated background region. In E the lowest measured value was used as background.

To show that the region of lower fluorescence in the middle of the phragmoplast is where the CP is, we stained membranes in GFP-TUA cells with the red fluorescing FM4-64. Indeed the central line of decreased GFP fluorescence coincides with an elevation of red signal (see fig. 4 C and F). As the cells were still alive >24 hours later and also undergoing cytokinesis their viability was not significantly reduced due to the FM4-64 treatment.

By tracking EB-1 comets we could see the behaviour of MT plus ends around the CP. In fluorescence intensity plots of EB1 like in 5 the CP can hardly be distinguished or not at all. Often it can be recognized only in time lapse images because the comets in the two halves move in opposite directions. Figure 6 shows nine cuts through the phragmoplast perpendicular to the CP. The diagonal lines in 6 A are the tracks of EB1 comets moving towards the CP. Notice that there is no space is left between the two pools moving in opposite directions. Except for one recording however no comets can be seen crossing through the CP, continuing their path in the opposite half. The elevated concentration of EB1 close to/in the CP region was recorded before by Bisgrove et al. 2008 but not discussed any further.
Figure 5 shows the average intensity of fluorescence of the mCherry and GFP across the phragmoplast and CP. Proximal to the CP EB1 levels are highest, while TUA is most abundant in both halves at a distance of ca. 2µm from the CP. Figure 7 shows that when the CP is cut by the confocal plane at a shallow angle, the difference between GFP-TUA and mCherry-EB1 is also visible.

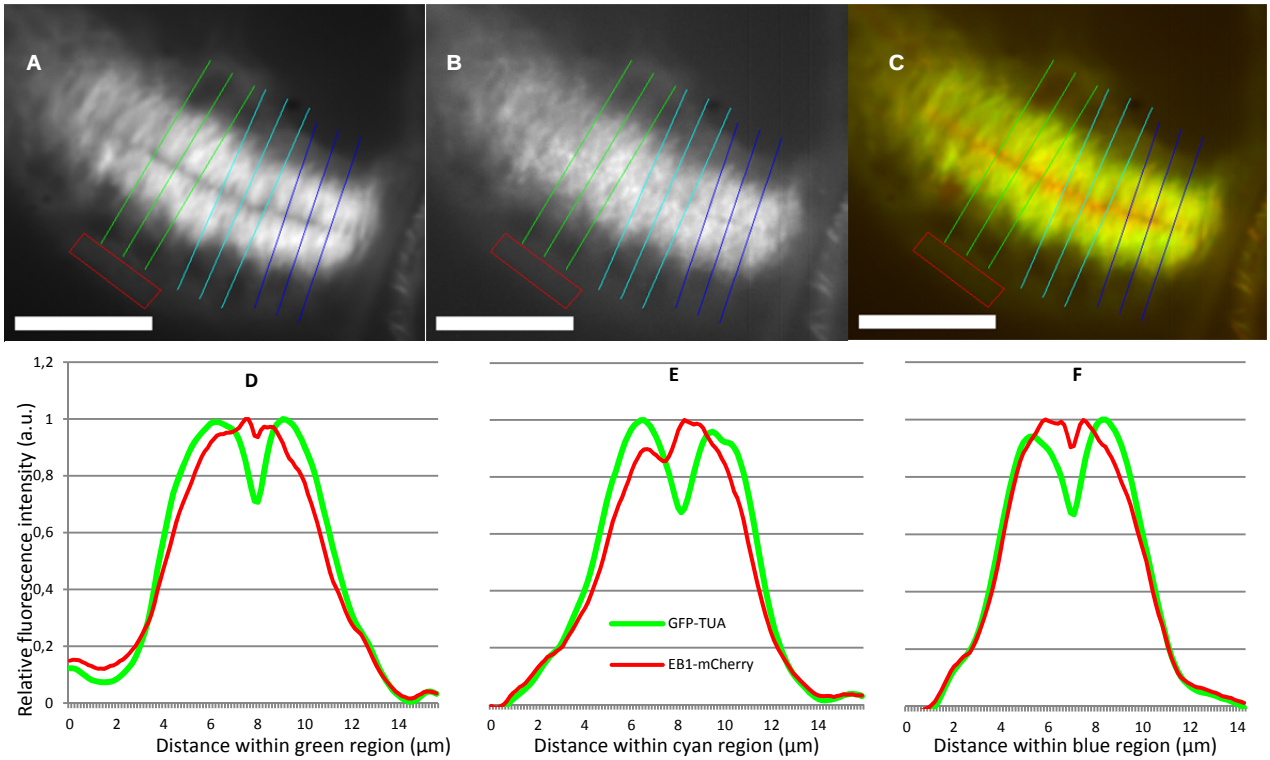

Figure 5. α plane view of a phragmoplast and signal intensity plots.
The averaged intensity of 156.7 sec.(72 frames) of a phragmoplast of a GFP-TUA_mCherry-EB1 cell. **A)** GFP-TUA signal; **B)** mCherry-EB1; **C)** Composite of A and B in green and red respectively; **D-F)** fluorescence signal intensity plots of the green, cyan and blue regions in A-C. Intensity within the red square was used a background signal. Contrast was managed per channel. Scale bar is 10µm.

The difference of absence of GFP-TUA and mCherry-EB1 around the CP could be an artefact, caused by different factors. Since the signal within every point of a recorded results not only from fluorescence in the corresponding spot in the specimen, but also in part from refracted light from the surrounding region, the discrepancy observed might result from differences in the amount of fluorescence surrounding the CP region. Next, the minimal size of objects that can be discriminated within a specimen depends, among others, on the wavelength of the light used and is therefore different for GFP (smaller) than it is for mCherry (larger size).

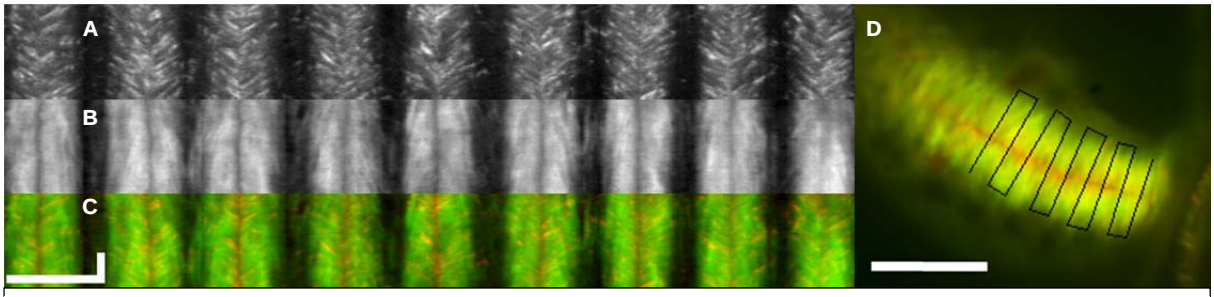

Figure6 A,B,C) Kymographs of mCherry-EB1, GFP-TUA and composite of A en B in red and green respectively along black line in D. D) α view, average intensity image of a phragmoplast. Scale bar is 10 µm for D. Scale square is 10µm wide and 50 sec high.

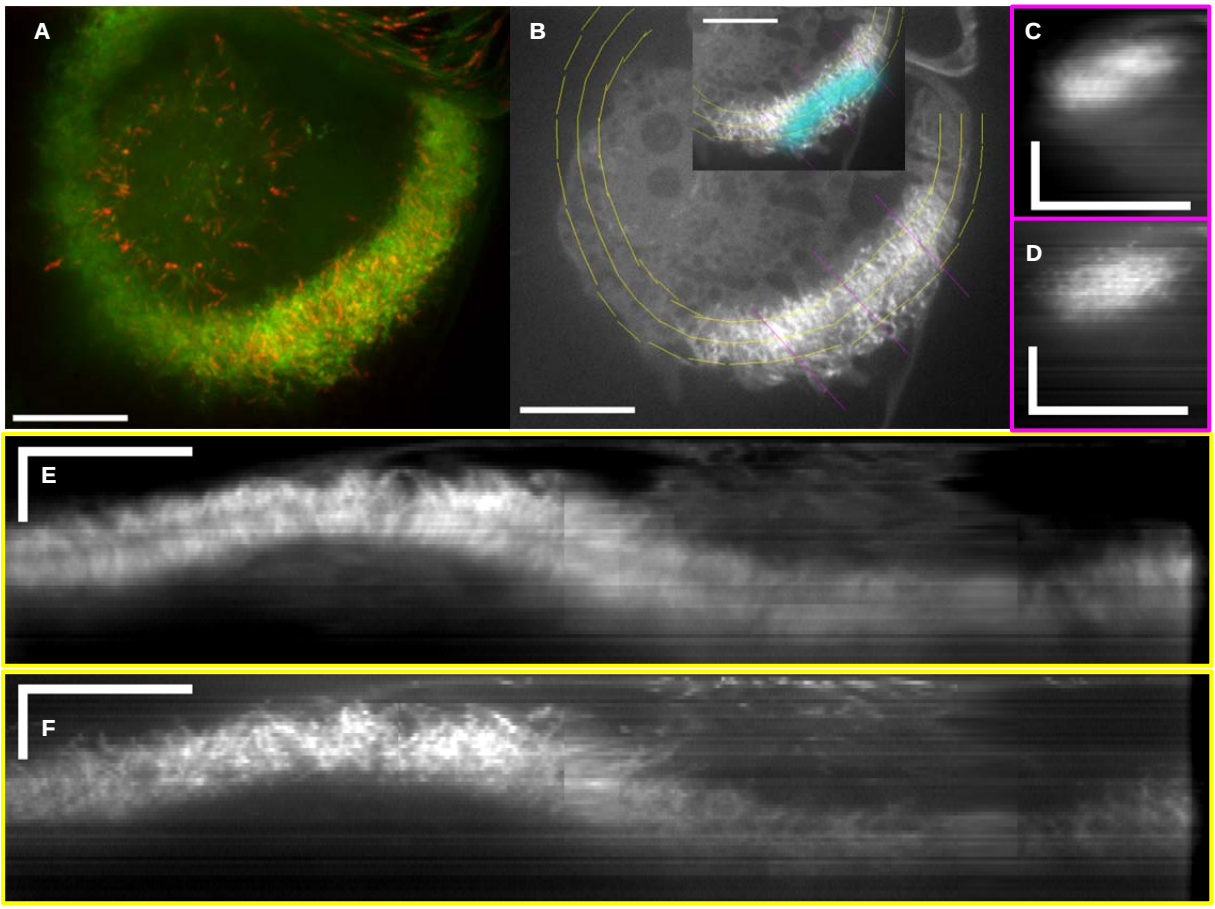

Figure 7. The dark region in between the MTs of the two phragmoplast halves is also visible in a δ like view while the border between EB1 is not.

A) projection over a depth of 23.5µm or 48 snapshots of a GFP-TUA_mCherry-EB1 phragmoplast positioned with an angle of 25˚ between the plane of view and the cell plate. **B)** Single frame of GFP-TUA signal. The magenta and yellow lines indicate kymograph areas for C,D and E,F respectively. **B inset**) fragment of B with the transient cyan region indicating were the dark region is visible between the two phragmoplast halves as the plane of views cuts through it. **C,D)** kymograph along the magenta lines in B (width is 200pxl=10.75 µm) of GFP-TUA and mCherry-EB1 respectively. The product is a β view like image. In C a dark region is visible separating the upper from the lower half, whereas in D no dark region can be distinguished. For clarity kymograph height is stretched 4x relative to width. **E,F)** kymograph (also stretched 4x height) along yellow lines in B (width is 68 pxl=3.65µm) from right to left. Also here the dark region in between the two halves is visible for GFP-TUA but not for mCherry-EB1. Scale bar=10µm. Scale square =10µm X 10µm.

We explored the possible influence of both these compromising factors on the accuracy of our observation by designing possible, simplified fluorescence signal profiles for GFP-TUA and mCherry-EB1 and simulating different convolutions of these profiles as they might occur in the microscope. The result is figure 8.
We investigated if a possible light refraction in the z direction also effected the observed width of fluorescence absence. For this we looked at a phragmoplast oriented at an angle of ca. 25° relative to the confocal slice. In this view the narrow CP is not cut at an angle of 90° but at 24° and hence should become visible as a broad bark region instead of narrow band. If the difference between GFP-TUA and mCherry-EB1 is not visible here, than in the other observations it must be an artefact. In this observation the same difference is apparent indeed.
The presumed GFP-TUA distribution consists of a region of homogenously elevated signal with a width of 5 µm for each halves of the phragmoplast separated by a 500 nm gap without signal. The mCherry-EB1 signal is similar except for two 500 nm wide peaks of double intensity next to the gap. Convolving an image or profile with a function like the ones used leads to a result in blurring of the image.
Convolution with airy distributions for 600 nm and 1000nm wavelength (yellow light colour and infra-red resp.) resulted in profiles in which the gap in the middle is still very clear for both GFP-TUA and mCherry-EB1. This means that the observed difference in CP width and depth cannot be caused by the different colours of the markers.
The influence of the surrounding fluorescence intensity by light refraction was mimicked by using broader airy distributions. Convolution with an airy distribution based on a wavelength of about 3-4 µm leads to a signal output resembling the fluorescence profiles observed (figure 5). With this convolution the gap in the GFP-TUA profile is still visible but the two peaks of the mCherry-EB1 profile prevail over the gap in between. A blur like this cannot cause the observed differences however. When convolution with such a wide airy distribution is

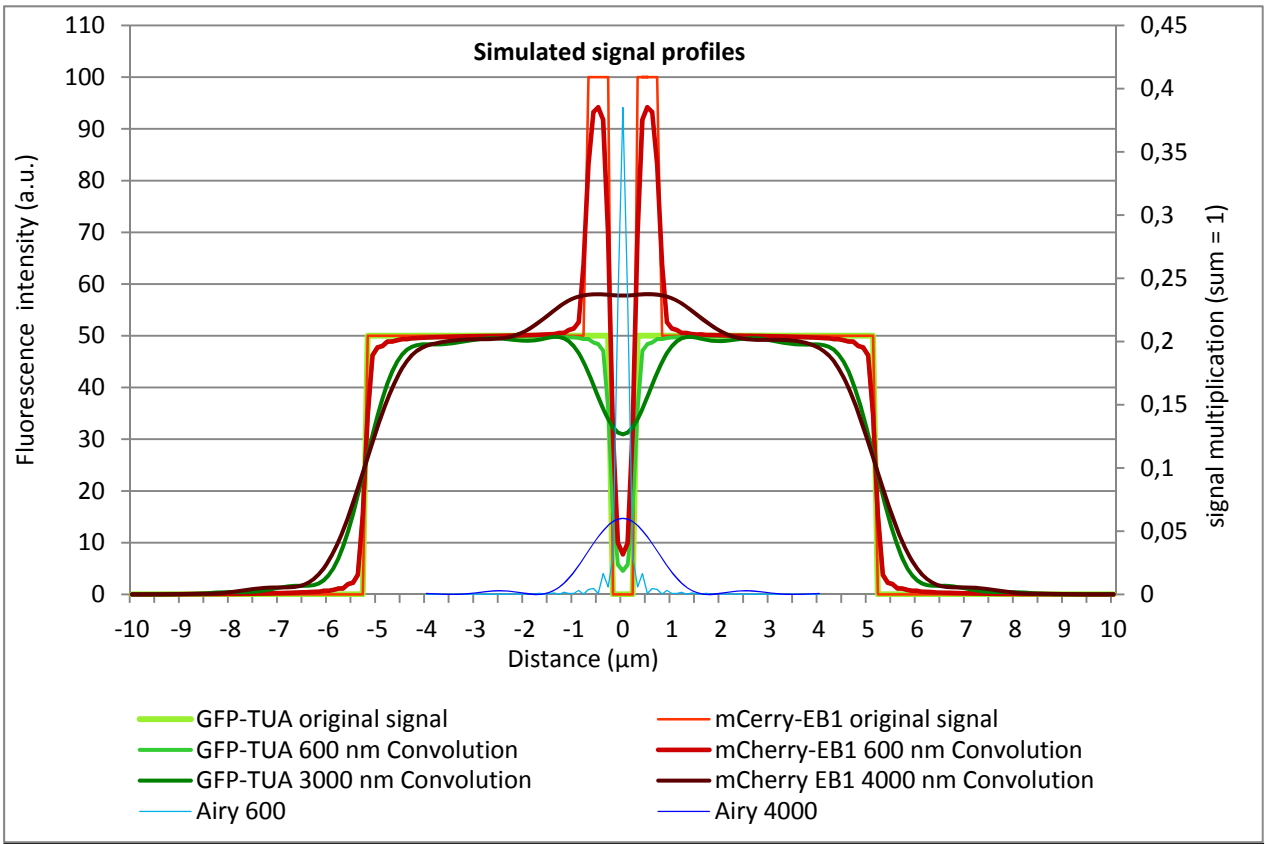

Figure 8 simulated effect of convolution on theoretical signal distribution.
The light-green and orange lines are theoretical distributions of GFP-TUA and mCherry-EB1 across the phragmoplast. The other green and red lines are simulated output distribution (left Y axis applies) .Blue lines are the airy distributions for 600 and 4000 nm. (The right Y axis applies)

applied to a punctate profile (data not shown), resembling a group of EB1 comets, the punctae loose there height and become so broad that the ones near to each other become indistinguishable. Such an effect is in conflict with our observations.
We must here for conclude that the difference between GFP-TUA and mCherry-EB1 really arises from an actual difference within the cell and that it is not an artefact. This suggests that EB1 moves further towards the CP then MTs do and even moves into the CP while MTs terminate at the CP surface or distance away from it.

MTs do grow around the CP edge

In contrast to the central parts of the phragmoplast the MTs at the (centrifugal) edge do grow through the division plain (outside of the CP) in to the realm of the other phragmoplast half. Often the growth of a such a MT is initially directed centrifugal, but diverges after crossing the division plain, and becomes more centripetal. Figure 9 depicts three MTs crossing the division plain beyond the CP edge. The extended parts of two of these MTs move lateral just after crossing each other. The comets in figure 10 show the deviation from there prior coarse, shortly after reaching the opposite phragmoplast half.

Flux

Within both the halves of the phragmoplast the fluorescence is not distributed homogeneously. Instead lighter and darker stripes roughly perpendicular to the CP give the impression that individual MTs or MT bundles can almost be distinguished (see 4 and 9 fig.). Time-lapse recordings show a movement of these MTs away from the CP (see figure 12). The speed of this receding movement has an average of 2.1 µm*min^{-1} (SE= 0.144, n=86) but differs between regions and shows a negative correlation to the distance to the CP ($p < 0.01$ in a non-parametric test.) When an area of 5X5 µm or bigger is photo bleached the same pattern of distal oriented

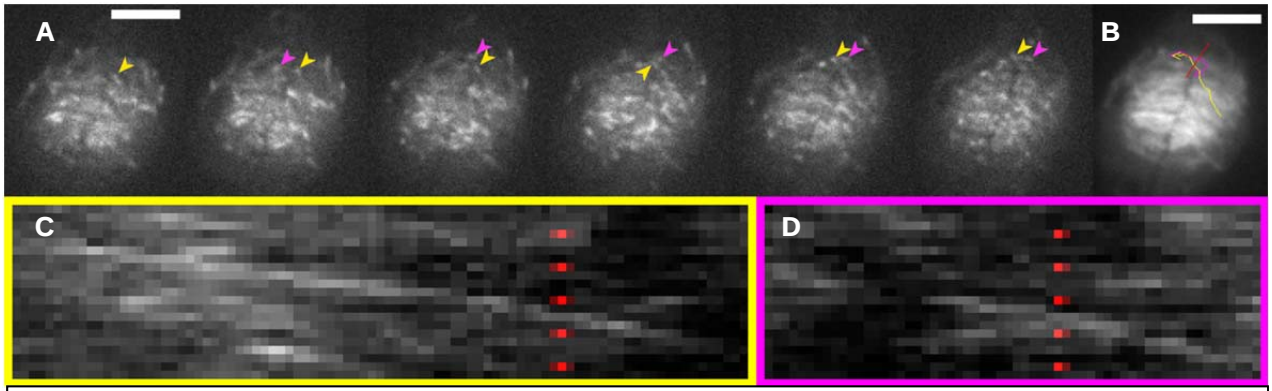

Figure 10 Two EB1 comets cross cell plate plane . **A)** Time series in β plane of EB1 comets. The cell plate (not visible) stretches towards the bottom left and is expanding towards the upper right. Yellow and magenta arrowheads point to two EB1 comets that cross each other while they move in to the opposite domains of the phragmoplast. **B)** Average intensity image of 70 seconds (21 frames) with the trajectories of the two kymographs C and D of the EB1 comets. The red line corresponds to the red dots in C en D and roughly indicates the cell plate plane. **C,D)** The kymographs along the lines in B for the same 21 frames as in B show the two comets crossing each other at a point on the red line in B. Scale bars =5 µm. time interval=3.34 seconds.

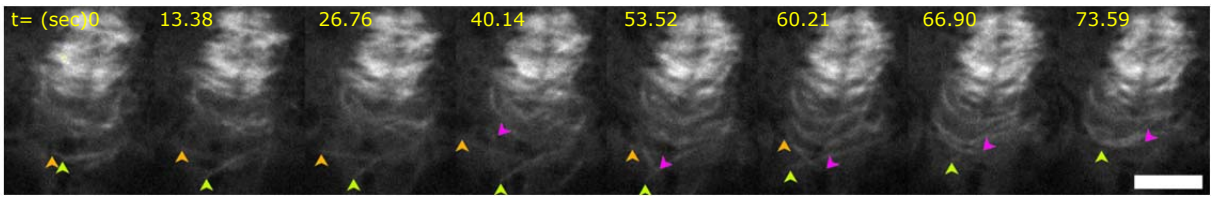

Figure 9 Three MTs cross division plane in cortex of a GFP-TUA cell. β plane view in the cell cortex. The tips of two MTs (indicated by yellow and green arrowhead) move from the right half of the phragmoplast towards the left while one MT (magenta arrowhead) grows in the opposite direction. The MT indicated by the green arrowhead remains directed away from the phragmoplast and wiggles about till the moment the magenta MT crosses it. Directly hereafter the green MT moves laterally into the rest of the phragmoplast. At t=66.90 at the site of overlap fluorescence intensity is increased. Scale bar = 5µm. Please notice that the time interval between frames is not constant.

movement can be seen even more clearly.
The movement seems to result, at least in part, from a oscillations of parts of the MTs or MT bundles. The oscillations move towards the MT minus ends and increases in amplitude, resulting in a wave like motion receding from the CP. See figure 11
In one time lapse recording the a single MT can be seen moving away from the CP while its plus end grows towards the CP at an angle of ± 33°. In the same recording at least two more MTs or thin MT bundles move away from the CP in a similar matter. These observations are incidental but clear. In other recordings the same process seems to occur, however these recordings show to little detail to be sure about the interpretation of the observed.

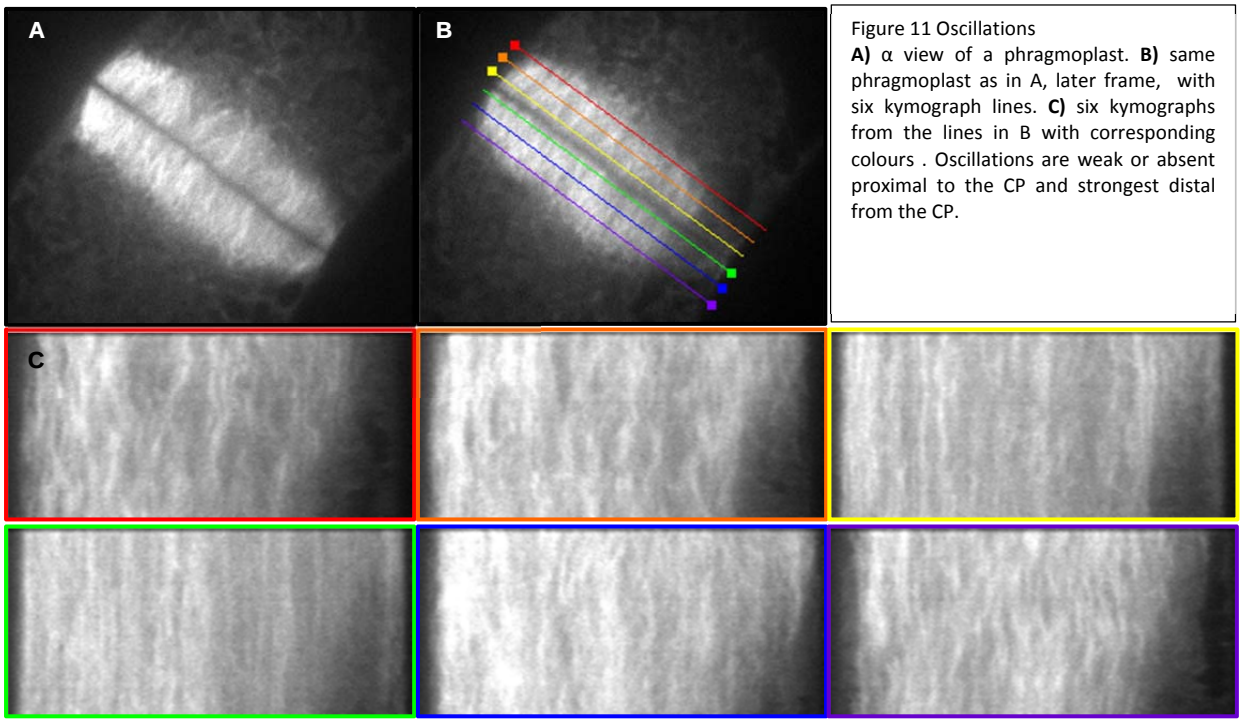

Figure 11 Oscillations
A) α view of a phragmoplast. **B)** same phragmoplast as in A, later frame, with six kymograph lines. **C)** six kymographs from the lines in B with corresponding colours . Oscillations are weak or absent proximal to the CP and strongest distal from the CP.

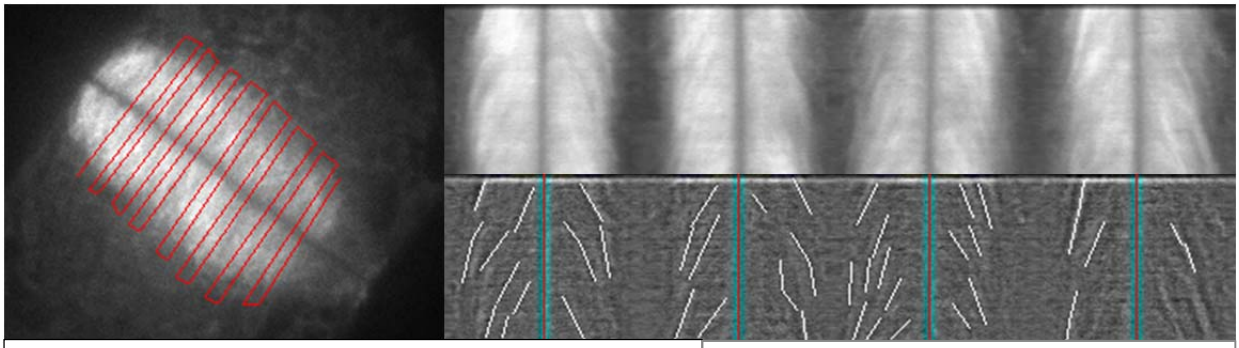

Figure 12. Relation between observed flux speed and distance to cell plate. **A)** β view of a phragmoplast with in red a kymograph line. **B)** Fragment from the kymograph from the red line in A, showing four cuts through the phragmoplast. The narrow dark vertical lines correspond to the CP and the light areas to MTs. The outward flux within the unevenly fluorescent phragmoplast, appears here as slightly lighter and darker lines directed downward away from the CP line. **C)** Modification of B used for further analysis. Contrast is locally increased to elucidate the flux lines. White lines are used for analisis of speed and distance **D)** scatter plot of the flux speed, and the distance to the cell plate.

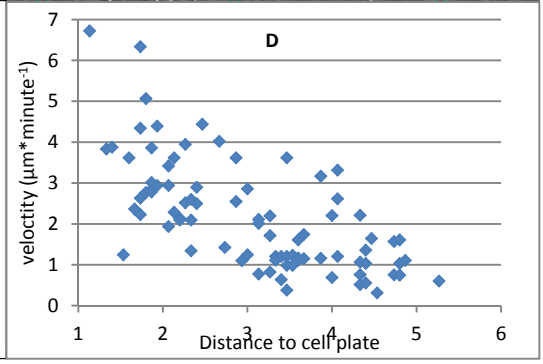

Fluorescence Recovery After photo-bleaching occurs in different fashions.

When a band with a diameter of 2µm, parallel to the CP is bleached an inconsistent set of recovery patters appears. Roughly four different ways of recovery can be observed. The recovery patterns are designated pattern 1 to 4 (see figure 13 A and B). In pattern 1 the distal edge of the band remained steady while the edge proximal to the CP moved towards the outer edge, thus narrowing the band. Pattern 2 shows a distal movement of the whole band, with the proximal border moving faster than the distal. When the band becomes narrower from both sides we speak of pattern 3. Pattern 4 is when the band fades, bud recovery does not seem to come from a certain direction. Pattern two is most dominant making up 39.6% (SE= 2.9%) of the recorded patterns. Within a single FRAP line multiple patterns can by occur.

Ratios of the first three patterns were compared between different regions of the phragmoplast (see figure 14). The fourth pattern occurred so infrequent that it was combined with recoveries that could not be

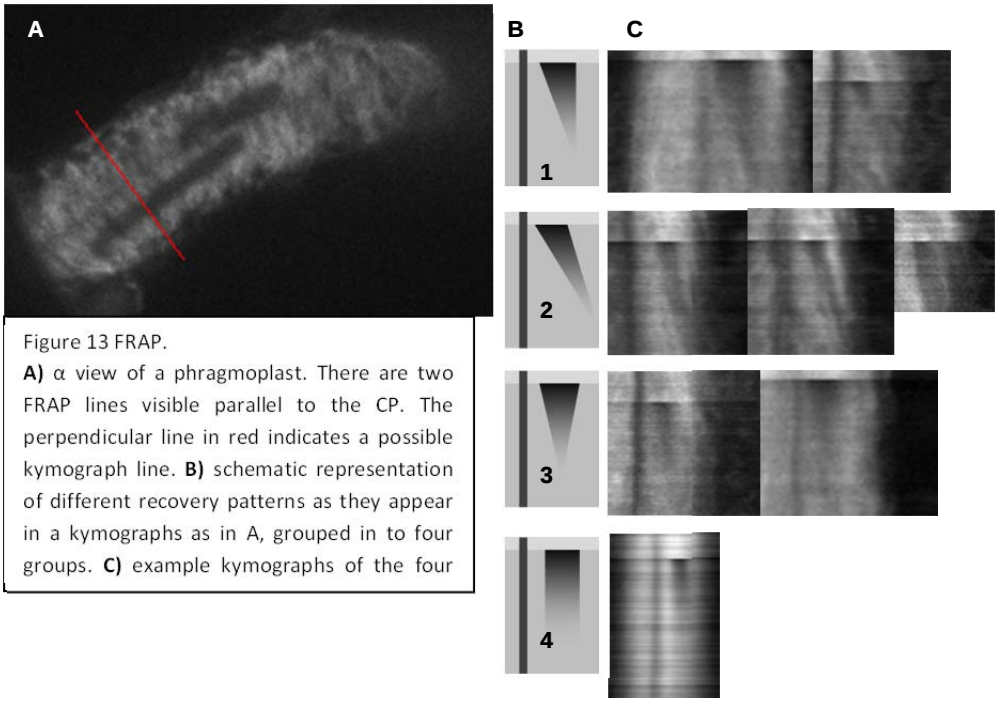

Figure 13 FRAP.
A) α view of a phragmoplast. There are two FRAP lines visible parallel to the CP. The perpendicular line in red indicates a possible kymograph line. **B)** schematic representation of different recovery patterns as they appear in a kymographs as in A, grouped in to four groups. **C)** example kymographs of the four

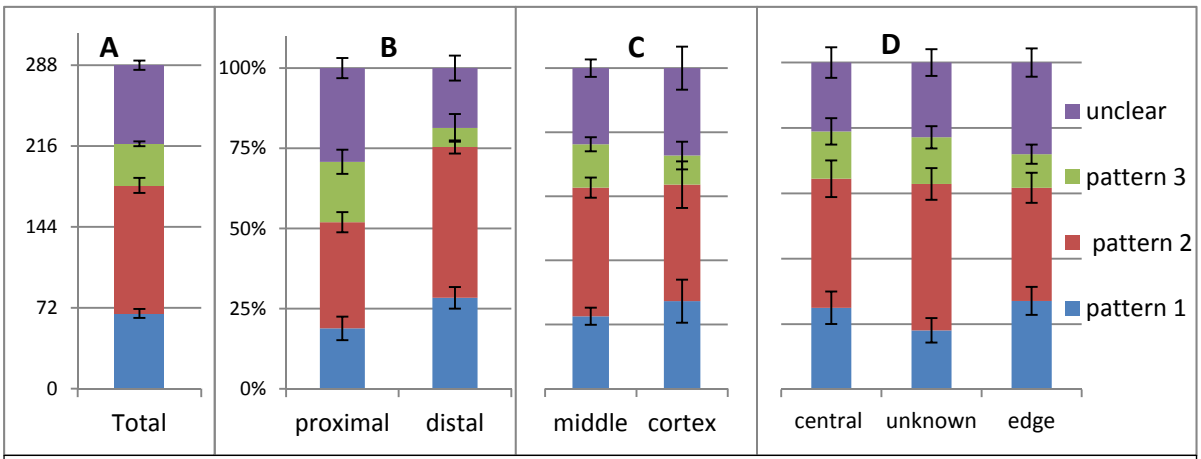

Figure 14 ratios between FRAP patterns and phragmoplast regions.
A-D) ratios of FRAP patterns 1,2,3 and patterns that were uncategorysable plus pattern 4. Error bard indicate SE. legend from D applies to A-D. **A)** absolute numbers. **B-D)** percentages per indicated region. Regions as depicted in figure 1.

designated to either of the patterns. No difference were apparent between the central part of the phragmoplast and the centrifugal edge. Proximity to the cell cortex did not seem to have a significant influence on the distribution of recovery patterns either. Proximal to the CP a significantly higher fraction of pattern 3 was recorded than distal from the CP ($p<0.0006$). The proximal fraction of pattern 3 is 18,8 % (SE=3.6%) against 6.0% (SE=2.0%) distal from the CP.

MTs grow faster in the phragmoplast than in the cortex

MT growth speed within the phragmoplast was established by tracking EB1 comets. Speed was calculated from kymographs of 165 EB-1 comets that remained in focus for at least 7 consecutive frames (minimal 9.75 seconds) in 7 different cells. The average growth speed is 7.8 µm/minute (SE= 0.128). The minimal and maximal recorded speed are 4.1 and 11.4 µm/min.

The growth speed in the phragmoplast is significantly higher compared to the speed found in the cortex ($p<0.0005$ Independent samples Mann Whitney U test), with a mean difference of 2.6 µm/minute (SE= 0.152)

Table XXX00X MT growth speeds

	Mean speed (µm/min)	SE	N	Mean Difference with former	SE	Significance p<
Cortex GFP-TUA	4.404	0.095	153	N/A	N/A	N/A
Cortex GFP-TUA_mCherry-EB1	5.179	0.085	236	0.774	0.120	0.0005
Phragmoplast GFP-TUA_mCherry-EB1	7.799	0.128	165	2.621	0.152	0.0005

Phragmoplast MTs do not all grow perpendicular to the CP

MTs approach the CP at wide range of angles with little or no parallelism, see figure 15. The average observed angle of approach is 61° (SE=1.66, n=155). The minimum angle of growth was 4° meaning that this comet

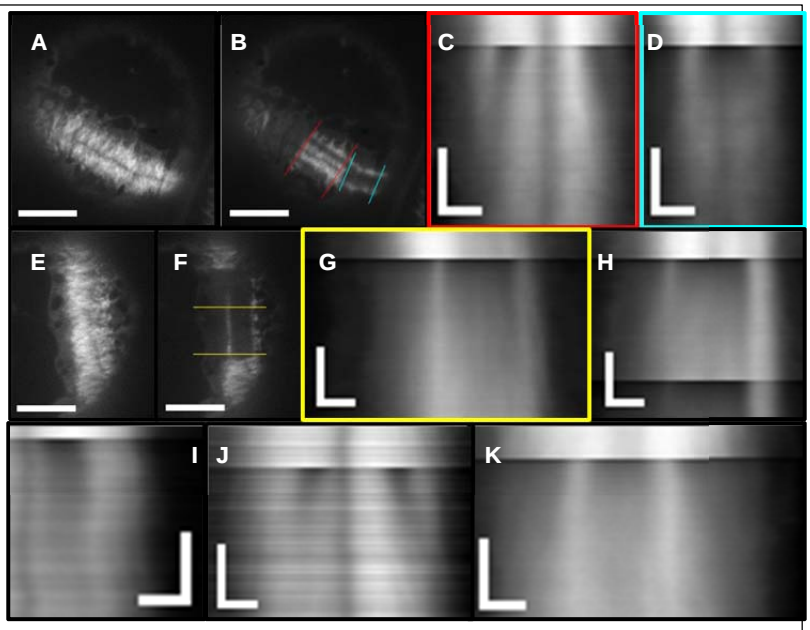

Figure 15. Broad kymographs. **A,B)**α view of phragmoplast before and just after photo bleaching. Lines in red and cyan delineate the lateral borders of two kymograph regions for C and D. Between, and perpendicular to, the red lines two narrow bands are bleached. **C)** Kymograph of region between the red lines in B. **D)** kymograph of the region between the cyan lines in B. **E,F)** α view on the outer edge of a phragmoplast, just before and immediately after bleaching. Yellow lines delineate the borders of the kymograph region for G. **G)** kymograph of region between yellow lines in F. **H)** Kymograph of roughly the same region as G, recorded some minutes later. **I,J)** In I a type 1 recovery and in J an unclear (either 1 or 2) and type 2 recovery. Kymographs with a large width. **K)** kymograph of IFRAP in same region as D. The two light bands do not diverge

moved practically parallel to the CP. The angles are based on straight lines between the two extremes of the kymograph lines used to establish MT growth speed. Because the used kymograph lines were somewhat longer than the actual trajectories (± 0.5 µm at both ends) this could have influenced the calculated angles.

Our impression is that growth directions have a centrifugal bias, especially on the centrifugal edge. This was not verified by quantification however.

In addition to the comets that could be followed, there were many visible for shorter times. Many of the these comets showed little movement. The time these dots remained visible corresponded to the time that would be expected for a comet crossing the plain of view at steep angle.

MTs do not grow straight

During MT growth in the phragmopalst EB1 comets regularly change direction. These changes can be subtle, covering a large part of the trajectory or can be rapid as can be seen in figurexxx0014 A. The changes in direction can go together with formation of curved MTs, as was observed a limited number of times, or might result from a combination of growth and lateral movement of the MT. The latter option was not taken in to account for calculation of the MT growth speeds.

The orientation of the change in direction did not seem to have an obvious relation to the distance to the CP, thought MTs seem to be bend so that the plus ends are more perpendicular to the CP and the minus end are more oblique and directed towards the phragmoplast centre, or possibly the nucleus.

A relation between growth speed and growth angle was investigated for a subset of 73 growth trajectories but was not found.

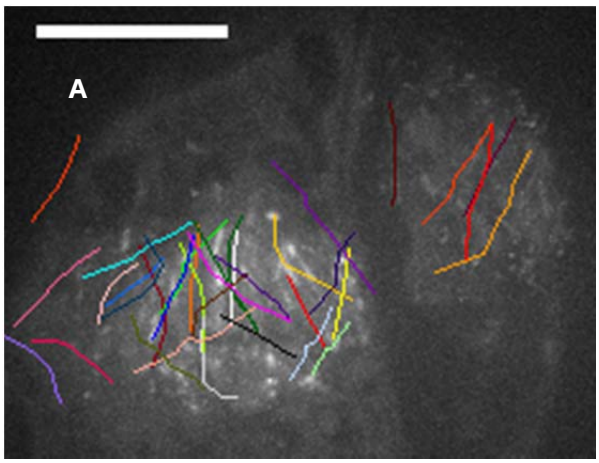

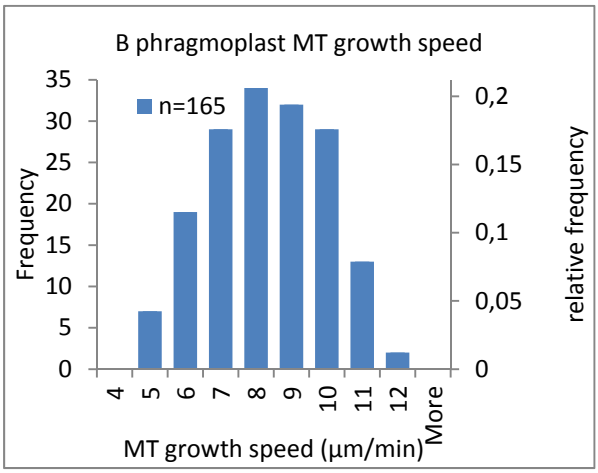

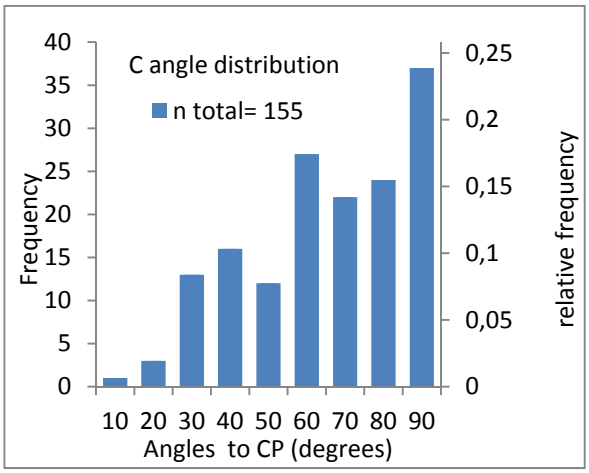

Figure 15 A) a view of phragmoplasts of two adjacent cells. Coloured lines indicate tracks of EB1 comets remaining in focus for at least 7 consecutive frames. Scale bar is 10 µm. **B)** MT growth speed distribution. **C)** Distribution of angles between EB1 comet trajectories or MT growth direction and CP. Scale bar = 10µm.

Phragmoplast expansion

There are two probable ways in which MT dynamics may contribute to Phragmoplast expansion.

Lateral, centrifugal movement of MTs at a pace similar to CP expansion results in expansion of the phragmoplast as a whole. The other possibility is that expansion results from net addition of MTs on the centrifugal edge, while there are fewer MTs growing on the central edge than there are disappearing. Literature leaves us to believe that the latter is the case (Assaad; Segui-Simarro et al., 2004), but

compelling evidence is not presented to our knowledge. Kymographs in figure xx007 show that expansion does indeed takes place primarily by the addition of MTs on the centrifugal edge. Images these kymographs are based on were taken at intervals of around 2.5 seconds. New MTs are visible as newly appearing lighter parts on consecutive horizontal cross sections. In the consecutive sections the majority of these lighter parts remain roughly at a constant position, thus forming vertical lines. Hence we can conclude that MTs or MT bundles do not deviate from their original location within the phragmoplast, throughout extended periods (up to at least 10 minutes) of phragmoplast expansion.

Initially the MTs or MT bundles seem to shiver or wave around. As the MT bundles grow thicker this movement can not be seen anymore. Towards the end the bundles become narrower again and the waving movement reoccurs.

Just before the central part of the phragmoplast in figure 16 I-L disappears EB1 is still present in that region. As the phragmoplast expands further, comets keep appearing at the very edge of the legging, centripetal sides. This indicates that the breakdown of the phragmoplast at this side must result from an increase in breakdown of MTs, rather than from a lack of growth.

16 H shows lateral movement of MTs in the direction of phragmoplast expansion. We did not establish the frequency of this type of event ,nor it's importance to phragmoplast expansion, but our impression is that it is of minor importance.

REACHING OUT TO CORTEX

In figure 17 some MT of the part of the phragmoplast that is magnified in xxx015B are reaching out toward the part of the cortex that is perpendicular to the plain of view. Two MTs or bundles can be seen exerting force. In the caption the analysis is explained. The size of the forces was not calculated. A situation like this, were the MTs reach out towards the cortex, was not recorded in other cells were the phragmoplast was equally close to the cortex and can not be considered representative.

As seen it figure 9 MTs do seem to influence each other when meeting around the CP edge however and the buckling of MTs like in figure 17 C,E,G is seen more often at the CP edge.

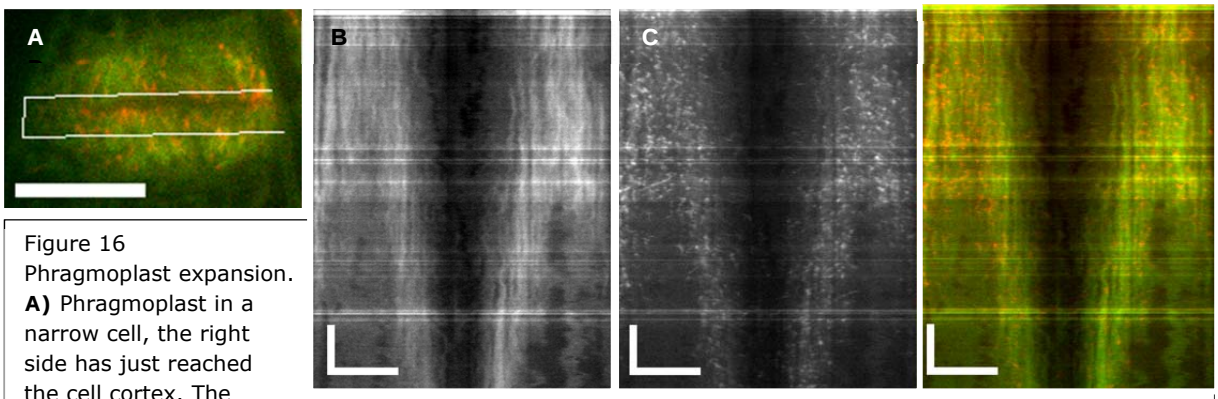

Figure 16
Phragmoplast expansion. **A)** Phragmoplast in a narrow cell, the right side has just reached the cell cortex. The white kymograph line reaches the cell cortex on both sides **B,C,D)** kymographs of A (GFP-TUA signal, mCherry-EB1 signal, composite). Horizontal scale bar is 10µm. Vertical scale bar is 100 seconds.

DISCUSSION

Different MT growth rates

MT growth speed seems to be influenced by the EB1 construct. This effect is not unexpected. EB1 is reported to have an effect on MT dynamics (Manna et al., 2008). Records were on different days in the sub culturing cycles however, hence viability might have varied between experiments and influenced the outcome.

Speed of EB1 comets in the phragmoplast shows much variation, but on average EB1 movement is much faster here than it is in the cortex. The high growth rate can partly be attributed to the constant proximity and thereby high availability of tubulin for growing MTs. Furthermore MT dynamics might be influenced by microtubule associate proteins (MAPs) that are specifically up regulated during this part of the cell cycle. The wide variation of MT growth direction is conflicting with the dogma of (strictly) parallel MTs e.g. [Wick 1991]

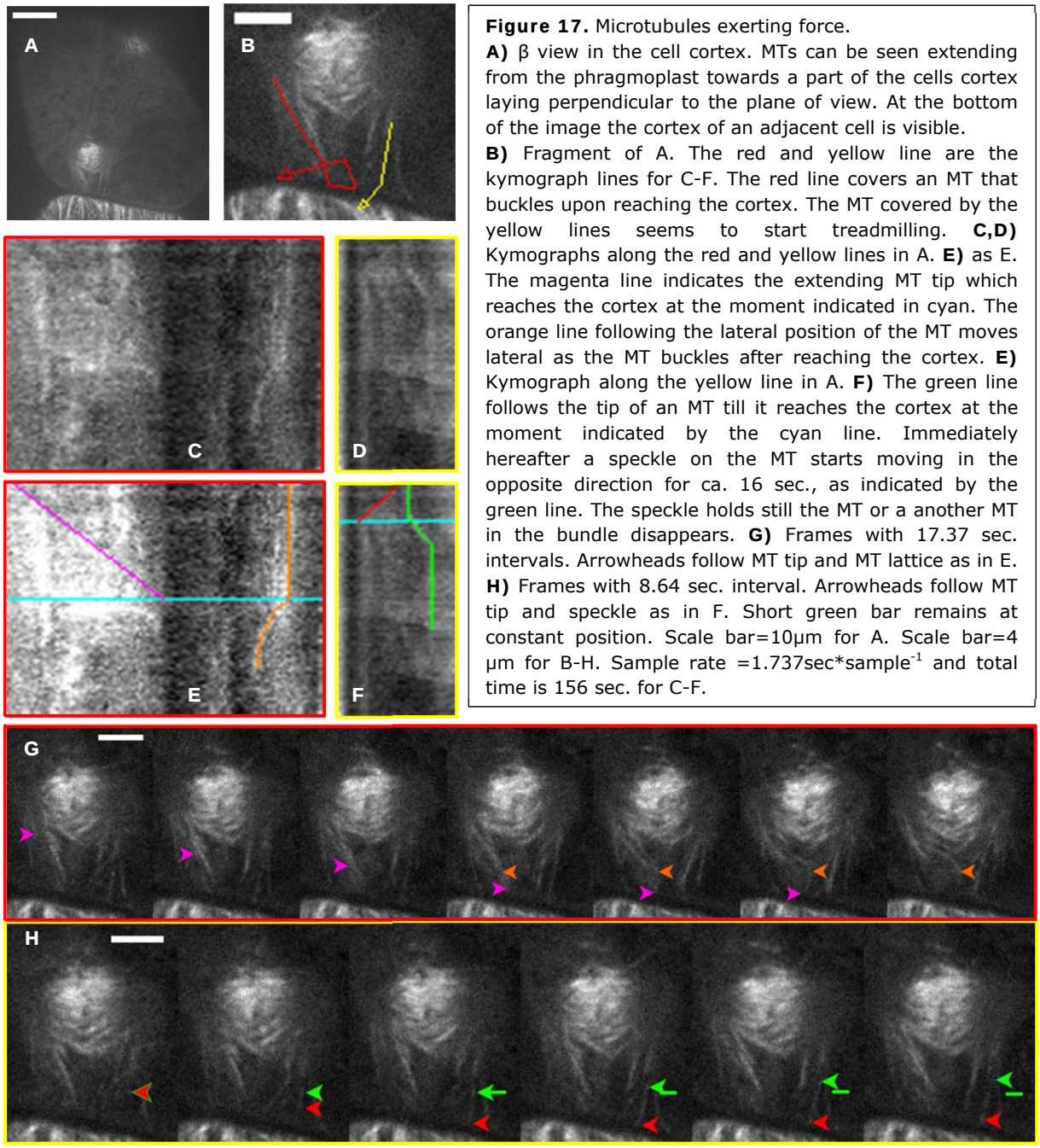

Figure 17. Microtubules exerting force.
A) β view in the cell cortex. MTs can be seen extending from the phragmoplast towards a part of the cells cortex laying perpendicular to the plane of view. At the bottom of the image the cortex of an adjacent cell is visible.
B) Fragment of A. The red and yellow line are the kymograph lines for C-F. The red line covers an MT that buckles upon reaching the cortex. The MT covered by the yellow lines seems to start treadmilling. **C,D)** Kymographs along the red and yellow lines in A. **E)** as E. The magenta line indicates the extending MT tip which reaches the cortex at the moment indicated in cyan. The orange line following the lateral position of the MT moves lateral as the MT buckles after reaching the cortex. **E)** Kymograph along the yellow line in A. **F)** The green line follows the tip of an MT till it reaches the cortex at the moment indicated by the cyan line. Immediately hereafter a speckle on the MT starts moving in the opposite direction for ca. 16 sec., as indicated by the green line. The speckle holds still the MT or a another MT in the bundle disappears. **G)** Frames with 17.37 sec. intervals. Arrowheads follow MT tip and MT lattice as in E. **H)** Frames with 8.64 sec. interval. Arrowheads follow MT tip and speckle as in F. Short green bar remains at constant position. Scale bar=10μm for A. Scale bar=4 μm for B-H. Sample rate =1.737sec*sample^{-1} and total time is 156 sec. for C-F.

Recovery patterns indicate motility

Significant differences

From the different FRAP patterns we concluded that the direction of MT movement within the phragmoplast is variable. Frequencies of the different movements are largely unrelated to the locations of the phragmoplast or to the proximity of the cell cortex however. Only a recovery directed toward the CP is recorded more often close to the CP then farther away from it. This movement is likely caused by plus end growth, or by motor induced plus end directed sliding of MTs.

The most abundant patterns

The most abundant pattern shows movement of the bleached area away from the CP. Remarkably the movement of the distal edge of the bleached band is often slower than the movement of the inner edge.

This pattern can be caused by treadmilling of MTs at different rates. When a number of MTs does not move at all, this result in the distal edge of a bleached area standing still, like in pattern one. It is not said however that this has to be the only reason for the constant bleach-fluorescence edge in pattern one to occur.

Other factors effecting FRAP

Pattern four, showing no direction of recovery is hard to explain in terms of MT kinetics.

This pattern can result from MTs slowly moving into the recorded region. This can happen by lateral displacement of the individual MT or by displacement of the phragmoplast. In case of movement in the z direction however the same effect would be expected to occur over a large distance of a FRAP band. Movement of the phragmoplast would likely be noticed however, resulting in exclusion of the record from FRAP analysis. The constant expansion of the phragmoplast would not cause movement of MT parts since expansion happens by the addition of new MTs on the centrifugal edge and not by lateral movement of the phragmoplast or individual MTs therein.

Movement of free tubulins in the cytosol likely causes the first rapid recovery in any of the records. Movement of other object in the cytosol can be responsible for a part of the observed flux and direction of recovery in all patterns.

Wide kymograph effect

Since fluorescence recovery can result from any event leading to the reappearance of active GFP-tagged tubulins in the bleached region and because the recovery of all these events are averaged in a wide kymograph the patterns in these kymographs are very hard to interpret. Because in a narrow kymograph fewer MTs fit, narrow kymographs likely represent single MT dynamics better.

Interdigitation

Asada et al.'s [1991] findings are in conflict with ours in two aspects. Asada presumes interdigitation of phragmoplast MTs in the CP region, based on literature, whereas we assume no interdigitation except during the transition phase from spindle to phragmoplast when the CP is not yet present and later on around the centrifugal edge. We expect the impression of interdigitation to arise in previous literature from overexposed imaging with a low amount of detail mostly due to low resolution techniques. Also images taken from the very edge and from very young phragmoplasts could produce the impression of ubiquitous overlap of MTs and interdigitation. Vantard (1990) shows interdigitation in lysed *Heamanthus* cells.

In Asadas and Vantard's experiments interdigitation might have resulted from sever cell manipulations such as the destruction of the cell walls, permeabilization of the membranes and anti-tubulin imunostaining of MTs. These manipulations might influence the interactions among MTs and their interaction with the CP.

Based on the fact that we see hardly any EB1 comets crossing the CP we conclude that in the in vivo situation in BY2 cells this interdigitation only happens incidentally. Electron microscopy (EM) work is somewhat conflicting here. Amongst others Assaad et al., [2001], Shopfer and Hepler [1991] and Segui Simaro et al., [2004] report MTs to cross through the CP, but images presented by Shopfer and Hepler [1991] and segui simaro et al.,

[2004] shows the far majority of MTs to terminate outside the CP and the images shown by the latter show the few MTs that do penetrate the CP not to be close enough to each other to expect physical linkage. The amount of interdigitation could also be species specific and dependant on the type of cell formation (somatic or gametophytic).
From the lateral movements of MTs that grow around the CP edge we conclude that these MTs interact with the MTs they encounter at the other half.

FLUX
Asada reports a flux of MTs directed away from the CP with a speed of 0.06 µm/min, presumable caused by mechano chemical enzymes. This is roughly 36 times slower than the flux we observe. We think this flux is another artefact, unrelated to the much faster flux we observe.
The differential flux speeds proximal to and distal from the CP can result from different ratios between treadmilling and not or slower treadmilling MTs. Also varying angles between the MTs and the direction in which the flux is measured can result in different impressions of flux speed. The waving motion can result from buckling of MTs as they grow and push against the CP.

Phragmoplast expansion
Expansion of the phragmoplast can be attributed to the addition of new MTs on the outer edge of the phragmoplast and not to centrifugal lateral displacement by MTs present in the phragmoplast. In literature both ways are assumed to be true [assaad 2001] and consensus is claimed [segui simaro 2004] but to our knowledge no previous records are presented anywhere with a sufficient imaging rate and resolution to actually elucidate the process of expansion at a scale from single MTs to MT bundles.
The enduring presence of EB1 comets in the central, legging part of the phragmoplast implies that disappearance of the phragmoplast in this region is caused by an increase in MT breakdown, rather than by decrease of MT formation in combination with an equal rate of MT breakdown.

Implications of intensity distributions for actual distribution.
The gradual variation of GFP-TUA between the CP end the phragmoplast distal edges indicates that not all MT ends of the same sort lie within one plane. While this might be expected for the growing MT plus ends, it is might be considered less obvious for the minus ends as the distal edge seems to maintain a constant distance to the CP over larger widths.

Acknowledgement
I would like to thank my supervisors Tijs Ketelaar, Marcel Janson and Jelmer Lindeboom for their persistent advices on my thesis work. The rest of the Plant Cell Biology chairgroup of Wageningen UR for their various advices help. I also want to thank the dutch government and my mother for supplying financial aids.

Literature references
(incomplete)

Akhmanova A, Hoogenraad CC (2005) Microtubule plus-end-tracking proteins: mechanisms and functions. Current Opinion in Cell Biology **17:** 47-54
Akhmanova A, Steinmetz MO (2010) Microtubule plus TIPs at a glance. Journal of Cell Science **123:** 3415-3419
Asada T, Sonobe S, Shibaoka H (1991) MICROTUBULE TRANSLOCATION IN THE CYTOKINETIC APPARATUS OF CULTURED TOBACCO CELLS. Nature **350:** 238-241
Assaad FF (2001) Plant cytokinesis. Exploring the links. Plant Physiology **126:** 509-516
Brøndsted HV, Carlsen FE (1951) A cortical cytoskeleton in expanded epithelium cells of sponge gemmules. Experimental Cell Research **2:** 90-96
Carlier M-F, Pantaloni D (1997) Control of actin dynamics in cell motility. Journal of Molecular Biology **269:** 459-467

Cassimeris LU, Walker RA, Pryer NK, Salmon ED (1987) DYNAMIC INSTABILITY OF MICROTUBULES. Bioessays **7:** 149-154

De Loof A, Broeck JV, Janssen I (1996) Hormones and the cytoskeieton of animals and plants. *In* International Review of Cytology, Vol 166, pp 1-58

Dogterom M, Yurke B (1997) Measurement of the force-velocity relation for growing microtubules. Science **278:** 856-860

Goto Y, Ueda K (1988) MICROFILAMENT BUNDLES OF F-ACTIN IN SPIROGYRA OBSERVED BY FLUORESCENCE MICROSCOPY. Planta **173:** 442-446

Hussey PJ (2011) The cytokinetic Phragmoplast: structure, proteomics, evolution and cytoskeletal copmonent. RMS Botanical Microscopy Meeting 2011

Lindemann CB, Orlando A, Kanous KS (1992) The flagellar beat of rat sperm is organized by the interaction of two functionally distinct populations of dynein bridges with a stable central axonemal partition. Journal of Cell Science **102:** 249-260

Manna T, Honnappa S, Steinmetz MO, Wilson L (2008) Suppression of microtubule dynamic instability by the plus TIP protein EB1 and its modulation by the CAP-Gly domain of p150(Glued). Biochemistry **47:** 779-786

Pickett-Heaps JD, Gunning BES, Brown RC, Lemmon BE, Cleary AL (1999) The cytoplast concept in dividing plant cells: Cytoplasmic domains and the evolution of spatially organized cell division. American Journal of Botany **86:** 153-172

Reichardt I, Stierhof Y-D, Mayer U, Richter S, Schwarz H, Schumacher K, Jürgens G (2007) Plant Cytokinesis Requires De Novo Secretory Trafficking but Not Endocytosis. Current Biology **17:** 2047-2053

Samuels AL, Giddings TH, Staehelin LA (1995) CYTOKINESIS IN TOBACCO BY-2 AND ROOT-TIP CELLS - A NEW MODEL OF CELL PLATE FORMATION IN HIGHER-PLANTS. Journal of Cell Biology **130:** 1345-1357

Sawitzky H, Grolig F (1995) PHRAGMOPLAST OF THE GREEN-ALGA SPIROGYRA IS FUNCTIONALLY DISTINCT FROM THE HIGHER-PLANT PHRAGMOPLAST. Journal of Cell Biology **130:** 1359-1371

Segui-Simarro JM, Austin JR, White EA, Staehelin LA (2004) Electron tomographic analysis of somatic cell plate formation in meristematic cells of arabidopsis preserved by high-pressure freezing. Plant Cell **16:** 836-856

Tanenbaum ME, Medema RH (2010) Mechanisms of Centrosome Separation and Bipolar Spindle Assembly. Developmental Cell **19:** 797-806

Van Damme D (2009) Division plane determination during plant somatic cytokinesis. Current Opinion in Plant Biology **12:** 745-751

Vos JW, Dogterom M, Emons AMC (2004) Microtubules become more dynamic but not shorter during preprophase band formation: A possible "search-and-capture" mechanism for microtubule translocation. Cell Motility and the Cytoskeleton **57:** 246-258